



Synthesis of water-soluble Ni(II) complexes and their role in photo-induced electron transfer with MPA-CdTe quantum dots

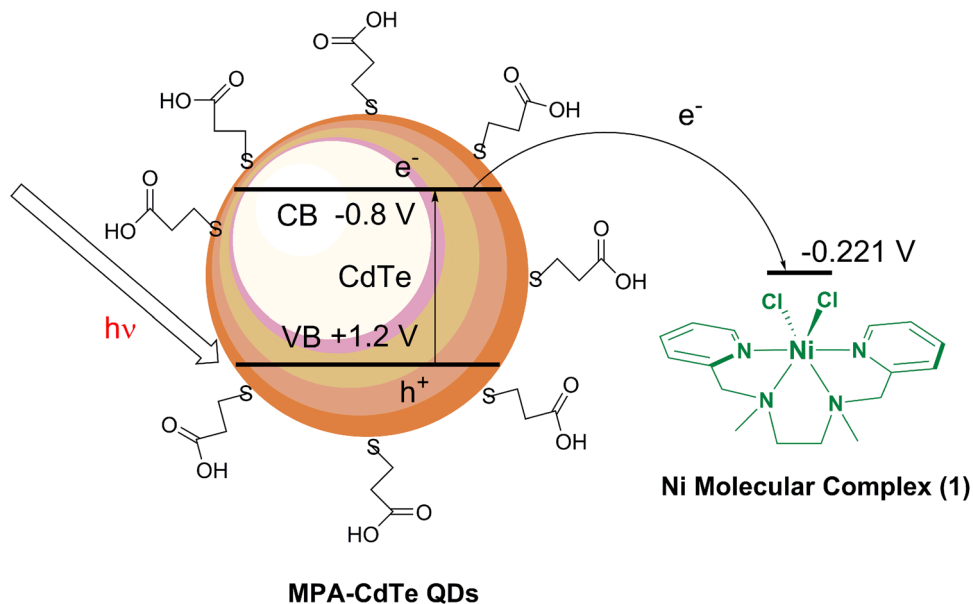
Niharika Krishna Botcha¹ · Rithvik R. Gutha² · Seyed M. Sadeghi² · Anusree Mukherjee¹

Received: 31 May 2019 / Accepted: 13 August 2019
© Springer Nature B.V. 2019

Abstract

Photocatalytic water splitting using solar energy for hydrogen production offers a promising alternative form of storable and clean energy for the future. To design an artificial photosynthesis system that is cost-effective and scalable, earth abundant elements must be used to develop each of the components of the assembly. To develop artificial photosynthetic systems, we need to couple a catalyst for proton reduction to a photosensitizer and understand the mechanism of photo-induced electron transfer from the photosensitizer to the catalyst that serves as the fundamental step for photocatalysis. Therefore, our work is focused on the study of light driven electron transfer kinetics from the quantum dot systems made with inorganic chalcogenides in the presence of Ni-based reduction catalysts. Herein, we report the synthesis and characterization of four Ni(II) complexes of tetradentate ligands with amine and pyridine functionalities (N₂/Py₂) and their interactions with CdTe quantum dots stabilized by 3-mercaptopropionic acid. The lifetime of the quantum dots was investigated in the presence of the Ni complexes and absorbance, emission and electrochemical measurements were performed to gain a deeper understanding of the photo-induced electron transfer process.

Graphic abstract



Electronic supplementary material The online version of this article (<https://doi.org/10.1007/s11120-019-00668-z>) contains supplementary material, which is available to authorized users.

Extended author information available on the last page of the article

Keywords Nickel complexes · Quantum dots · Photo-induced electron transfer · Biomimetic systems · Artificial photosynthesis

Abbreviations

AP	Artificial photosynthesis
QDs	Quantum dots
MPA	3-Mercaptopropionic acid
UV–Vis	Ultraviolet-Visible
K_{sv}	Stern–Volmer quenching constant
k_q	Bimolecular quenching rate constant
TCSPC	Time-correlated single-photon counting
E_g	Bandgap
E_{vb}	Valence band energy level
E_{cb}	Conduction band energy level
NHE	Normal hydrogen electrode
NMR	Nuclear magnetic resonance
ESI–MS	Electrospray ionization mass spectrometry
RT	Room temperature

Introduction

The increasing global demand for energy has compelled the need to look for a clean alternative source that is safe and sustainable like solar energy (Gust et al. 2001). The energy provided by the sun in an hour is more than that consumed by the world in a year (Wu et al. 2014). Solar energy has the unique potential to sustain the ever-growing energy needs of humanity in the most environmentally benign manner (Vullev 2011). However, the intermittent and diffuse nature of the sunlight mandates the need to store solar energy in a cost-effective way (Mulfort and Utschig 2016). Photosynthesis provides an excellent paradigm to store solar energy in the form of chemical bonds. This has inspired scientists to design artificial photosynthesis (AP) systems that will capture and convert solar energy to chemical energy by understanding the processes in natural photosynthesis and mimicking their solar energy conversion mechanisms in simple man-made models and systems, but with better efficiencies for future scale-up applications (Kaerkaes et al. 2014; Kalyanasundaram and Graetzel 2010; Kim et al. 2015; Mao and Shen 2013; Zhou et al. 2016). Over the past, several decades, several AP systems have been designed and developed for the utilization of sunlight and efficient production of solar fuels by mimicking the key structural elements and functions of natural photosynthesis (Utschig et al. 2015; Xu and Zhang 2015). The high specific enthalpy of combustion as well as water being the benign combustion product make H_2 an ideal solar fuel (Armaroli and Balzani 2007; Esswein and Nocera 2007; Wang and Li 2017; Wu et al. 2014).

There are three fundamental steps in an efficient AP systems: (i) charge separation in a photosensitizer due to the

absorption of light (ii) charge transfer from the photosensitizer to a catalyst; and (iii) chemical reactions driven by the redox potential stored in the catalyst to couple that electron transfer to chemical bond formation (Wang et al. 2015). To develop highly efficient artificial photocatalytic systems, the key issue to address is the right and effective combination of the photosensitizer and the catalyst (Wang et al. 2015). The photosensitizers must have good stability, broad spectral absorptions in the visible light region to maximize the use of solar energy, and long excited state lifetimes for effective charge separation. Early efforts on finding photosensitizers relied heavily on molecular light absorbers such as $[Ru(bpy)_3]^{2+}$ and other organic dyes such as fluorescein and eosin Y, however, in the past two decades quantum dots as potential light harvesters have garnered significant attention (Li et al. 2018). The advantages offered by quantum dots (QDs) include their unique size-dependent absorption properties, large absorption cross-sections over a broad spectral range, long exciton lifetimes and superior photostability (Gross et al. 2014; Liu et al. 2015; Sadeghi et al. 2018, 2019; Wu et al. 2014).

One of the strategies for sustainable artificial photosynthetic systems are homogeneous molecular catalytic systems with earth-abundant elements for the reduction of water because of their ease of synthesis, tunable redox properties and their cost-effectiveness (Artero and Fontecave 2013; Du and Eisenberg 2012; Fukuzumi et al. 2013; Wang et al. 2015). Over the past two decades, molecular catalysts, especially biomimetic complexes composed of earth abundant elements such as Fe, Co and Ni, have been developed and studied for the catalytic proton reduction for H_2 generation (Berardi et al. 2014; Wen and Li 2013; Xu and Zhang 2015). Particularly Ni-based molecular catalytic system supported by N2P2 ligands has shown excellent proton reduction capabilities under electrocatalytic conditions (Helm et al. 2011; Kilgore et al. 2011; Wilson et al. 2006, 2007). These successful DuBois catalysts have led to the design of several AP systems where Ni or its complexes were coupled to different light-harvesting materials (Gross et al. 2014; Silver et al. 2013).

In the last decade, there has been growing interest to design AP systems using QDs as photosensitizers and hydrogenases or their functional mimics as the catalysts in water (Brown et al. 2010, 2012; Gimbert-Surinach et al. 2014; Greene et al. 2012; Li et al. 2013a, b; Nann et al. 2010; Wang et al. 2011) Water-soluble CdTe QDs serve as excellent photosensitizers because of their high extinction coefficients as well as the intrinsic advantages they offer such as the high-photoluminescence quantum yields

and the quantum confinement effects (Gaponik et al. 2002; Gimbert-Surinach et al. 2014; Shi et al. 2006; Zhang et al. 2003). Specifically, the assemblies of MPA-CdTe QDs (or MPA-CdSe QDs) along with molecular catalysts in aqueous solutions are able to photocatalytically produce H_2 with exceptional activity and impressive durability under visible light irradiation (Huang et al. 2012; Wang et al. 2014; 2015; Wu et al. 2014; Zhou et al. 2017). However, most of these reports focus on performance of the photocatalytic system toward hydrogen production very little is known about the kinetics of photo-induced electron transfer, crucial for effective photocatalysis.

To improve efficiency of an existing AP system and to design the next-generation system, it is essential to understand the mechanism of photoinduced electron transfer from the photosensitizer to the catalyst. This understanding will ensure a proper design of an AP system that is a water-soluble, scalable and sustainable alternative. In the present work we report synthesis and characterization of four water-soluble mononuclear nickel complexes (Fig. 1) supported by tetradentate ligands with amine and pyridine functionalities (N₂/Py₂). Complexes 1–4 were carefully designed to tune their electronic and steric properties. In a separate study, we have shown that complexes 1 and 2 both can produce H_2 from proton reduction under electrocatalytic and photocatalytic conditions using organic and inorganic dyes

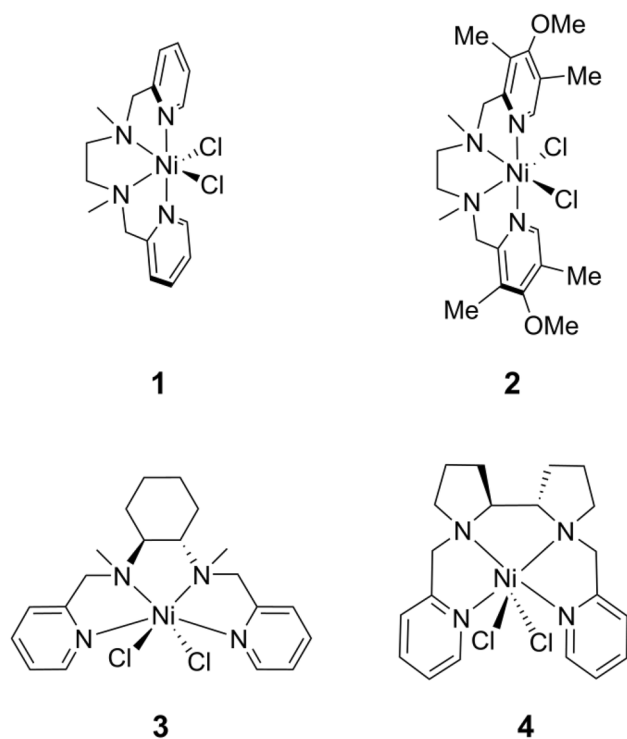


Fig. 1 Synthesized nickel complexes 1–4 with bispicen (N₂/Py₂) ligand system

(Kankanamalage et al. 2019). In the current work water-soluble CdTe quantum dots stabilized by 3-mercaptopropionic acid (MPA-CdTe QDs) were selected as the photosensitizer due to their aqueous dispersion and economical advantage (Li et al. 2013a; Wang et al., 2011). This work focuses on understanding the kinetics of photoinduced electron transfer of these QDs in the presence of complexes 1–4 to pave the way to develop a better multicomponent AP system comprising inorganic chalcogenide-based QDs and earth-abundant transition metal complexes.

Results and discussion

The syntheses of the ligands were performed by following the published procedures (Pella et al. 2018; Singh et al. 2017). Complexes 1–4 were synthesized by mixing equimolar amounts of the nickel salt with the respective ligands. In water, complexes 1–4 all gave faintly green-colored solutions with optical bands in the visible region with weak intensities (Fig. 2). All absorption data including the peak position and molar absorptivity are summarized in the Table 1.

The optical spectrum of complex 1 matches with previously reported spectral data (Singh et al. 2017). The spectral features of the complexes 1–4 are consistent with six-coordinate octahedral geometry for Ni(II) (Guadalupe Hernandez et al. 2006; Liu et al. 2012; Mautner et al. 2009; Singh et al., 2017). The band in the near-UV region is characteristic of an intra-ligand charge transfer transition (Anaconda et al. 2009). In the visible region, all the Ni(II) complexes exhibit two *d-d* bands with low intensities around 564–568 nm and 920–934 nm which can be adequately represented by the

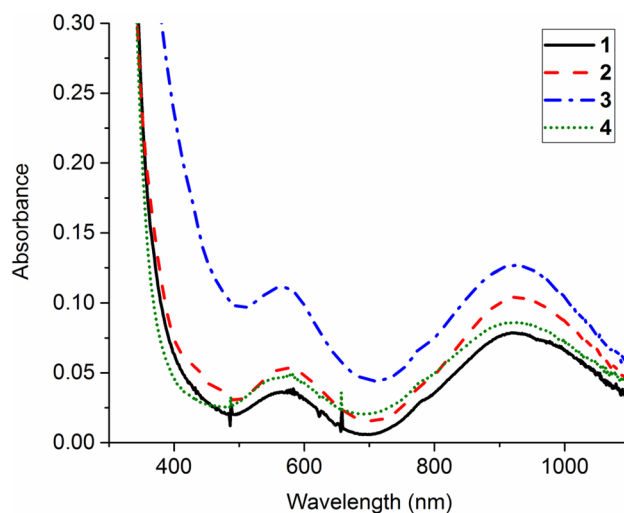


Fig. 2 Optical spectra of complexes 1 (black solid line), 2 (red-dashed line), 3 (blue dash-dotted line) and 4 (green-dotted line) in water using a quartz cuvette with 1 cm path length. All complexes are dissolved in water to give an 8 mM concentration

Table 1 Optical and electrochemical parameters for complexes **1–4**

Complex	Peak position λ_{\max} (nm)	Molar absorptivity ($M^{-1} \text{ cm}^{-1}$)	Peak position λ_{\max} (nm)	Molar absorptivity ($M^{-1} \text{ cm}^{-1}$)	Peak shoulder λ (nm)	E_{pc} versus NHE (V)
1	566	5	922	10	400, 790	−0.221
2	569	7	934	13	400, 790	−0.259
3	564	14	922	16	450, 790	−0.275
4	568	6	920	11	390, 790	−0.313

$^3A_{2g}$ to $^3T_{1g}$ (F) transition in the 550–800 nm range and the $^3A_{2g}$ to $^3T_{2g}$ (F) transition in the 850–1100 nm range (Gurumoorthy et al. 2016; Liu et al. 2012; Mautner et al. 2009; Sadhu et al. 2015; Singh et al. 2017). The optical spectra of the complexes **1–4** match reasonably well with the other reported complexes of high spin d^8 Ni(II) in an octahedral geometry (Singh et al. 2017).

The reduction potentials of the Ni complexes **1–4** were measured using cyclic voltammetry (Fig. S1a–d). The complexes were scanned from +1 V to −1 V in water with 0.1 M KCl as the supporting electrolyte with a scan rate varied from 100 to 500 mV s^{-1} . All four Ni complexes exhibited cathodic waves corresponding to the Ni(II)/Ni(I) reduction (Kankanamalage et al. 2019; Zilbermann et al. 2005) around −0.509 V versus Ag/AgCl for **1**, −0.547 V for **2**, −0.563 V for **3**, and −0.601 V for **4**, respectively, well within the range of other known Ni complexes. The potentials with respect to the normal hydrogen electrode (NHE) for the complexes **1–4** are listed in Table 1.

The MPA-CdTe QDs were characterized by measuring their UV–Vis absorption spectra and the luminescent spectra as shown in the Figs. S2 and S3, respectively (see SI). The concentration of the MPA-CdTe QDs was determined as 2.8×10^{-6} M (1 mg mL^{-1}) using the Beer–Lambert law (Fig. S2). On the basis of the absorption band centered at 620 nm, the particle size of the MPA-CdTe QDs was determined to be 3.9 nm using the Eqs. S1 and S2 (see SI) (Yu et al. 2003). The bandgap of CdTe is narrow (around 1.44 eV), and so all wavelengths of visible light provide sufficient energy for the excitation of the electrons (Amelia et al. 2012; Haram et al. 2011).

Luminescence quenching

The MPA-CdTe QDs exhibit absorption bands in the range of 550–650 nm (Fig. S2). The photoluminescence of the MPA-CdTe QDs were measured in water at room temperature following excitation at 514 nm. These QDs are luminescent at room temperature with emission maximum at 638 nm (Fig. S3). To probe impact of luminescent intensity upon addition of nickel complexes, solution of complexes **1–4** in water was added to the solutions of MPA-CdTe QDs. Optical spectra of the MPA-CdTe QDs upon

the addition of the Ni complex **1** (Fig. S4a) showed no remarkable changes suggesting that the structure and properties of the MPA-CdTe QDs were not impacted upon the addition of the complex. However, the emission intensity at 638 nm was dramatically quenched upon the addition of the complexes (Fig. 3).

Furthermore, the luminescence quenching could be directly correlated to the concentration of the complex **1** with maximum quenching to be observed with 500 equivalents. The concentration dependent quenching was further investigated using Stern–Volmer equation for **1**, that yielded a quenching rate constant of $5.4 \times 10^{10} \text{ M}^{-1} \text{ s}^{-1}$. Similar effects were observed for the other three nickel complexes **2**, **3** and **4**. In all the cases, optical bands of the QDs remain unchanged upon addition of the complex solution (Fig. S4b–d) but emission spectra showed steady decline in emission intensity (Fig. S5a–c). Table 2 lists the Stern–Volmer quenching constant K_{sv} and the bimolecular quenching rate constant k_q for all the complexes **1–4** (Fig. S6a–d). Stern–Volmer quenching constant for all the complexes are reasonably similar. Similarly, bimolecular rate constants for **1**, **2**, **3** and **4** are all in the same order further corroborating their similar potential as effective quenchers.

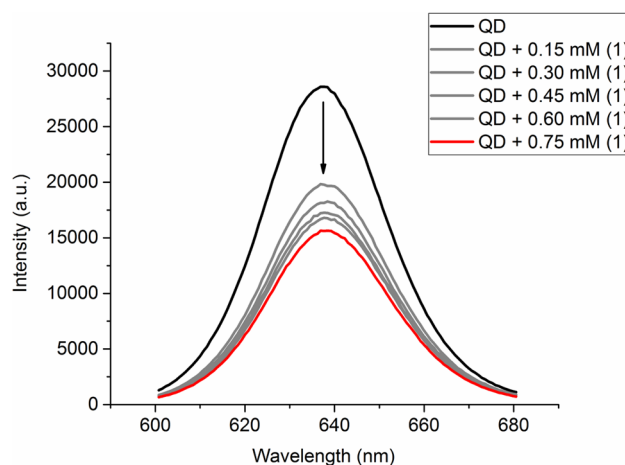


Fig. 3 Luminescence spectra of MPA-CdTe QDs (1.4×10^{-6} M, 0.5 mg mL^{-1}) with increasing concentration of complex **1** (0 to 0.75×10^{-3} M) in water (excitation wavelength: 514 nm)

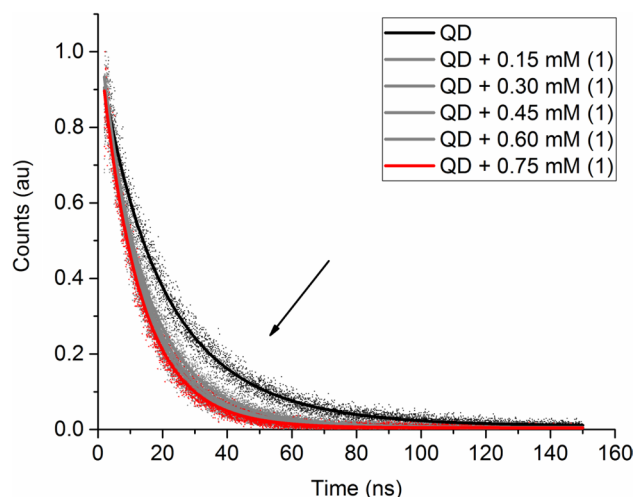
Table 2 The Stern–Volmer quenching constant K_{sv} and the Bimolecular quenching rate constant k_q for complexes **1–4**

Complexes	Stern–Volmer quenching constant K_{sv} (M^{-1})	Bimolecular quenching rate constant k_q ($M^{-1} s^{-1}$)
1	1.3×10^3	5.4×10^{10}
2	1.9×10^3	8.0×10^{10}
3	1.9×10^3	7.8×10^{10}
4	8.5×10^2	3.7×10^{10}

Luminescence decay

A number of processes could lead to the quenching, such as energy transfer, electron transfer or complex formation. Because of the minimal spectroscopic overlap of the absorption of the complexes **1–4** (Fig. 1) and the emission of the MPA-CdTe QDs (Figure S3), the quenching could not be attributed to the energy transfer process from the excited MPA-CdTe QDs to the complexes **1–4**. Therefore, the luminescence quenching most likely arises due to electron transfer from the excited MPA-CdTe QDs to the complexes **1–4**. To further corroborate the above data, we measured the luminescence lifetime of the MPA-CdTe QDs using time-correlated single-photon counting (TCSPC) system and monitored lifetime changes in the presence of Ni complexes. Analysis of the decay revealed that the luminescence lifetime of the MPA-CdTe QDs was shortened considerably with the progressive addition of the complexes **1–4** (Table 3). Since we observe a decrease in the lifetime of the MPA-CdTe QDs in the presence of the complexes **1–4**, we can eliminate the possibility of complex formation between them.

The decay lifetime was best fit by a biexponential function (Table S1a–d). The average lifetime of MPA-CdTe QDs in water at room temperature was 24 ns. It was observed that on the addition of the complex **1** to the solution of the QDs resulted in faster decay with concentration dependence suggesting electron transfer in the multicomponent molecular system with freely diffusing donors and acceptors (Fig. 4). It is observed that the lifetime of the QDs with the addition of **1** falls from 24 to 13 ns which is a decrease to almost half

**Fig. 4** The luminescence decay of MPA-CdTe QDs (1.4×10^{-6} M, 0.5 mg mL^{-1}) with increasing concentrations of complex **1** (0 to 0.75×10^{-3} M) in water (excitation wavelength: 450 nm)

of the original lifetime. All other complexes showed similar concentration dependence on the decay rate (Fig. S7a–c) and significant faster decay as summarized in Table 3. Therefore, in all the four cases the decay of the MPA-CdTe QDs in the presence of the nickel complexes **1–4** were almost twice as fast.

To establish that the photoluminescence quenching and luminescence decay rate are not a result of the concentration change of the QDs solution, experiments were performed where MPA-CdTe QDs solutions were diluted with the addition of water achieving the concentrations of 0.15 mM to 0.75 mM (Fig. S8a, b). These control experiments showed no appreciable change in the luminescence intensity of the MPA-CdTe QDs in the presence of added water. No significant quenching was observed upon addition of water, moreover no changes in lifetime decay in the absence of the complexes **1–4** (Table S2). These control experiments demonstrate that electron transfer from the QDs to the Ni complexes is responsible for the change in excited state dynamics as measured with the luminescence quenching and decay experiments.

Table 3 Mean lifetimes of the quantum dot in the presence of **1–4**

	Mean lifetime for 1 (ns)	Mean lifetime for 2 (ns)	Mean lifetime for 3 (ns)	Mean lifetime for 4 (ns)
QD	24	24	24	24
QD+0.15 mM	16	15	16	19
QD+0.30 mM	14	13	14	17
QD+0.45 mM	14	12	13	16
QD+0.60 mM	13	12	12	15
QD+0.75 mM	13	11	12	15

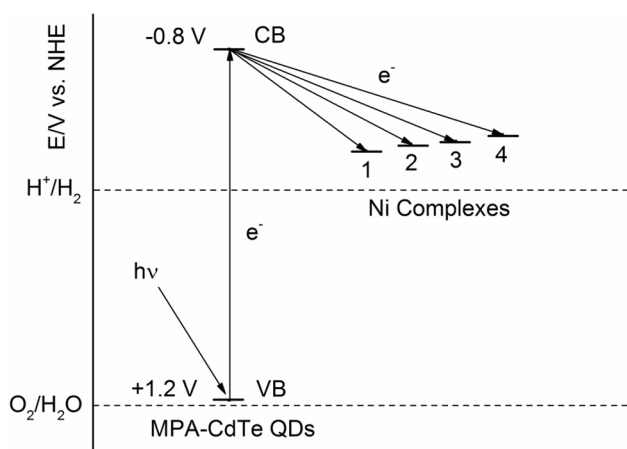


Fig. 5 Potentials (vs. NHE) of the excited MPA-CdTe QDs and the cathodic peak potentials (vs. NHE) of the complexes **1–4**

Therefore, the luminescence quenching and decay of MPA-CdTe QDs can be attributed to electron transfer from the excited MPA-CdTe QDs to the Ni complexes **1–4**. To further confirm this hypothesis, we used a combination of spectroscopic and electrochemical studies. The bandgap (E_g) calculated from the absorption spectra of the MPA-CdTe QDs is 2 eV (Fig. S2) (Bae et al. 2004; Gimbert-Surinach et al. 2014; Poznyak et al. 2005). The anodic peak potential of the MPA-CdTe QDs (Fig. S9) is +0.907 V versus Ag/AgCl, which gives an estimated value for the valence band energy level (E_{vb}) as +1.2 V versus NHE (Gimbert-Surinach et al. 2014; Rajh et al. 1993; Wang et al. 2011). Utilizing the values for E_{vb} and E_g , the calculated value for the conduction band energy level (E_{cb}) for the MPA-CdTe QDs is -0.8 V versus NHE (Gimbert-Surinach et al. 2014; Li et al. 2013a; Rajh et al. 1993; Wang et al. 2011). The cathodic peak potentials of the complexes **1–4** versus NHE are summarized in Table 1. Based on our findings, since the energy of the conduction band of the MPA-CdTe QDs is more negative than the cathodic peak potentials of the complexes **1–4**, electron transfer from the excited MPA-CdTe QDs to the Ni complexes **1–4** is energetically favorable (Fig. 5) (Li et al. 2014; Rajh et al. 1993).

Conclusion

The synthesis and characterization of a series of water-soluble mononuclear Ni(II) complexes supported by the N2/Py2 tetradentate ligand family were reported. Photoluminescence properties of this MPA-CdTe QDs system were investigated in detail in the presence of nickel complexes, to gain fundamental understanding about their prospects for potential photocatalytic systems. All Ni complexes **1–4** investigated in this paper showed promising results, they

were able to reduce lifetime of QDs suggesting that they can accept electrons from the quantum dots. Surprisingly, changing the ligand architecture by varying the donation property of the pyridine group (**1** vs. **2**) or having a rigid backbone (**1** compared to **3** and **4**) did not lead to significant change in the decay lifetimes (Fig. 5, Table 1). Future work includes the addition of the sacrificial electron donor to complete the three-component system and investigate whether the ligands have an impact on the amount of hydrogen produced, despite having similar effects in the photo-induced electron transfer rates.

Experimental section

Materials and methods

All reagents and solvents were purchased from Millipore-Sigma and Fisher Scientific and directly used for synthesis without further purification unless otherwise mentioned. 1,2-dimethylcyclohexane-1,2-diamine was obtained from Alfa Aesar. Water-soluble Cadmium telluride quantum dots stabilized by 3-mercaptopropionic acid (MPA-CdTe QDs) were purchased from NNCrystal US Corp. Deuterated solvents used for Nuclear magnetic resonance (NMR) spectroscopy were purchased from Cambridge Isotope Laboratories, Inc.

^1H NMR experiments were performed in deuterated solvents on a Varian Inova-500 MHz instrument at 25 °C. Electrospray ionization mass spectrometry (ESI-MS) experiments were performed on a Thermo Scientific LTQ Orbitrap XL Hybrid FT Mass Spectrometer in positive ionization mode. Elemental analyses were performed by Atlantic Microlab, Inc. (Norcross, GA). Electronic absorption spectra were measured on an Agilent Cary 8454 UV-Vis spectrometer in a quartz cuvette with a 5 mm path length. Electrochemical measurements were carried out on a BASi-C3 Epsilon electrochemical instrument using a glassy carbon working electrode, a platinum wire auxiliary electrode, and Ag/AgCl reference electrode. All cyclic voltammetry experiments were performed under nitrogen atmosphere using 0.1 M KCl as the supporting electrolyte. Graphical representation and data analysis were performed using Origin program.

The Emission spectra were recorded using a TE-cooled QEPRO spectrometer from Ocean Optics. A continuous wave laser diode with 514 nm wavelength was used as an excitation source. A combination of dichroic mirrors and filters were used to separate the emission of the quantum dots from the laser beam before sending it to the spectrometer. To measure the lifetime of the quantum dots, we used time-correlated single-photon counting (TCSPC) system (Picoquant Time harp 260) combined with 30-ps pulsed

laser with a 450 nm wavelength. All the above emission and lifetime measurements were performed with special optical glass cells with a pathlength of 10 mm.

Synthesis of *N,N'*-dimethyl-*N,N'*-bis-(pyridine-2-ylmethyl)-1,2-diaminoethane (BPMEN)

The ligand BPMEN was synthesized via a previously reported procedure (Singh et al. 2017). A solution of potassium carbonate (5.1 g, 37 mmol) in 15 mL water was dropwise added to the aqueous solution of 2-(chloromethyl)pyridine hydrochloride (3 g, 18.3 mmol in 10 mL). After about 30 min of stirring at room temperature, the reaction mixture was extracted with dichloromethane (3 × 20 mL). The combined organic extracts were dried over anhydrous sodium sulfate. The solution was filtered, and the solvent was removed under vacuum. The resulted residue was then dissolved in dichloromethane (10 mL). The above solution was added dropwise to a solution of *N,N'*-dimethylethylenediamine (0.942 mL, 8.75 mmol) in dichloromethane (25 mL). After this addition, 20 mL of aqueous sodium hydroxide (1 M) was added slowly and the reaction mixture was stirred for next 60 h at room temperature. After stirring was finished, another fraction of sodium hydroxide (20 mL, 1 M) was added rapidly. The reaction mixture was extracted with dichloromethane (3 × 50 mL) and the combined organic portion was dried over anhydrous sodium sulfate. Evaporation of solvent led to isolation of the ligand BPMEN as a dark orange oil. (2.1 g, Yield – 89%) ¹H NMR (500 MHz, Methanol-*d*₄) δ 8.45 (d, 2H, pyridine ring), 7.76 (m, 2H, pyridine ring), 7.52 (d, 2H, pyridine ring), 7.30 (m, 2H, pyridine ring), 3.67 (s, 4H, –N–CH₂–Py), 2.63 (s, 4H, –CH₂–CH₂–), 2.26 (s, 6H, N–CH₃). ESI–MS⁺: [BPMEN + H]⁺ = 271.15 m/z⁺ (experimental) 271.19 m/z⁺ (theoretical).

Synthesis of [*N,N'*-dimethyl-*N,N'*-bis-(4-methoxy-3,5-dimethylpyridine-2-ylmethyl)-1,2 diaminoethane. (345BPMEN)

The ligand 345BPMEN was synthesized by modifying the previously reported procedure (Singh et al. 2017). To a solution of 2-chloromethyl-4-methoxy-3,5-dimethylpyridine hydrochloride 2.032 g (9.15 mmol) in 10 mL of water, a solution of potassium carbonate (2.55 g, 18.45 mmol) in water (10 mL) was added dropwise. After potassium carbonate addition, very thick white ppts were formed and solution solidified. Additional amount of water (50 mL) was added into the mixture. After water addition, the reaction mixture was stirred at room temperature for next 30 min followed by solvent extraction with dichloromethane (3 × 20 mL). The combined dichloromethane layer was treated with anhydrous sodium sulfate. The solution was filtered, and the solvent was removed by rotatory evaporation. The collected

light brown oil was dissolved in dichloromethane (10 mL). The above solution was added dropwise to a solution of *N,N'*-dimethylethylenediamine 0.493 mL (4.58 mmol) in dichloromethane (15 mL). Aqueous solution of 1 M sodium hydroxide (10 mL) was slowly added and solution was stirred for additional 60 h at room temperature. After 60 h of stirring was the rapid addition of a second fraction of aqueous 1 M sodium hydroxide (10 mL, 10 mmol), the product was extracted with dichloromethane (3 × 25 mL). The combined organic layers were dried over anhydrous sodium sulfate and filtered. Subsequently, the excess solvent was evaporated by vacuum to afford brown color viscous oil (1.71 g, Yield 97%). ¹H NMR (500 MHz, Methanol-*d*₄) δ 8.08 (s, 2H, pyridine ring), 3.76 (s, 6H, –O–CH₃–Py), 3.57 (s, 4H, –CH₂–CH₂–Py), 2.56 (s, 4H, –CH₂–CH₂–), 2.28 (d, 6H, CH₃–Py), 2.24 (d, 6H, CH₃–Py), 2.16 (s, 6H, –N–CH₃). ESI–MS⁺: [345BPMEN + H]⁺ = 387.32 m/z⁺ (experimental) 387.27 m/z⁺ (theoretical).

Synthesis of *N1,N2*-dimethyl-*N1,N2*-bis(pyridin-2-ylmethyl)-cyclohexane-1,2-diamine (BPMCN)

The ligand BPMCN was synthesized via a previously reported procedure (Pella et al. 2018). Briefly, 1,2-dimethylcyclohexane-1,2-diamine (162 mg, 1.14 mmol) was dissolved in acetonitrile (15 mL) in a round-bottom flask. Triethylamine (0.78 mL, 5.6 mmol) was charged to the solution, and 2-(chloromethyl)pyridine (374 mg, 2.27 mmol) was added. The solution as brought to reflux in air overnight, then cooled to room temperature and condensed under reduced pressure. The resulting crude solid was dissolved in 30 mL of dichloromethane and washed with 30 mL of saturated sodium bicarbonate (aq). The organic layer was extracted, and the aqueous layer was washed 2 × 30 mL with dichloromethane. The organic layers were collected, dried over sodium sulfate, filtered, and condensed under reduced pressure to yield a brown oil. The crude product was purified using silica gel chromatography with 86% Ethyl acetate/10% Methanol/4% Ammonium hydroxide to yield the desired product as a light brown oil (0.15 g, Yield 41%). ¹H NMR (500 MHz, CDCl₃) δ 8.47 (d, 2H), 7.59 (d, 4H), 7.12 (m, 2H), 3.87 (q, 4H), 2.67 (d, 2H), 2.29 (s, 6H), 2.02 (2H), 1.73 (d, 2H), 1.29 (m, 2H), 1.17 (t, 2H). ESI–MS⁺: [BPMCN + H]⁺ = 325.31 m/z⁺ (experimental) 325.23 m/z⁺ (theoretical).

Synthesis (-)-2-(((S)-2-((S)-1-(pyridin-2-ylmethyl)pyrrolidin-2-yl)pyrrolidin-1-yl)methyl)pyridine (PDP)

The ligand PDP was synthesized via a previously reported procedure (Pella et al. 2018). A 100 mL round-bottom flask was charged with a stir bar, (S,S)-2,2'-bispyrrolidine tartrate

(S2) (0.25 equiv, 1.0 g, 3.45 mmol) and water (7.5 mL), and dichloromethane (7.5 mL). Solid sodium hydroxide pellets (1.6 equiv, 0.883 g, 22.05 mmol) were added, followed by 2-(chloromethyl)-pyridine (0.55 equiv, 1.243 g, 7.575 mmol). After 18 h stirring at room temperature, the reaction mixture was diluted with 1 M sodium hydroxide. The aqueous layer was extracted with dichloromethane (3×12.5 mL), and the organic extracts were combined, dried over magnesium sulfate, and concentrated in vacuo. The crude ligand thus obtained was purified by silica gel chromatography (5% Methanol/2% Ammonium hydroxide/Dichloromethane) and the collected fractions were combined, washed with 1 M sodium hydroxide, dried over magnesium sulfate, and concentrated in vacuo to provide a brown oil (0.515 g, Yield 46%). $^1\text{H NMR}$ (500 MHz, CDCl_3) δ 8.50 (dd, 2H), 7.60 (dt, 2H), 7.40 (d, 2H), 7.11 (dd, 2H), 4.20 (d, 2H), 3.51 (d, 2H), 3.00 (p, 2H), 2.80 (m, 2H), 2.24 (appq, 2H), 1.77–1.64 (m, 8H). ESI-MS⁺: $[\text{PDP} + \text{H}]^+ = 323.32$ m/z (experimental) 323.22 m/z (theoretical).

Synthesis of Ni(BPMEN)Cl₂ (1)

The complex **1** was prepared by following a published procedure (Singh et al. 2017). The ligand BPMEN (0.238 g, 1 mmol) dissolved in methanol (4 mL) was added dropwise to a stirring solution of $\text{NiCl}_2 \cdot 6\text{H}_2\text{O}$ (0.27 g, 1 mmol) in methanol (4 mL). Blue green solution was obtained immediately upon addition. Evaporation of solvent gave a blue green color powder (0.396 g, Yield 99%). ESI-MS (in CH_3OH) for $[\text{Ni}(\text{BPMEN})\text{Cl}]^+ (z=1)$ m/z 363.13 (experimental) m/z 363.09 (theoretical) and for $[\text{Ni}(\text{BPMEN})]^{2+} (z=2)$ m/z 164.21 (experimental) m/z 164.06 (theoretical). Elemental analysis Calculated (%): C 45.37, H 6.27, N 12.45 Found (%): C 45.18, H 5.82, N 13.3. UV-Vis λ_{max} in nm (ϵ in $\text{M}^{-1} \text{cm}^{-1}$) in MeOH at RT: 603 (15), 986 (26).

Synthesis of Ni(345BPMEN)Cl₂ (2)

The complex **2** was prepared by following similar procedure as reported for **1**. The ligand 345BPMEN (0.198 g, 0.512 mmol) dissolved in methanol (3 mL) was added dropwise to a stirring solution of $\text{NiCl}_2 \cdot 6\text{H}_2\text{O}$ (0.122 g, 0.512 mmol) in methanol (3 mL). The color of the solution turned immediately bluish green upon addition. Evaporation of solvent gave a blue green color powder (0.262 g, Yield 99%). ESI-MS (in CH_3OH) for $[\text{Ni}(345\text{BPMEN})\text{Cl}]^+ (z=1)$ m/z 479.25 (experimental) m/z 479.17 (theoretical) and for $[\text{Ni}(345\text{BPMEN})]^{2+} (z=2)$ m/z 222.26 (experimental) m/z 222.10 (theoretical). Elemental analysis Calculated (%): C 47.29, H 7.25, N 9.59 Found (%): C 47.56, H 6.69, N 10.42. UV-Vis λ_{max} in nm (ϵ in $\text{M}^{-1} \text{cm}^{-1}$) in MeOH at RT: 610 (16), 974 (28).

Synthesis of Ni(BPMCN)Cl₂ (3)

Addition of the ligand BPMCN (0.033 g, 0.1 mmol) dissolved in methanol (2 mL) to a stirring solution of $\text{NiCl}_2 \cdot 6\text{H}_2\text{O}$ (0.024 g, 0.1 mmol) in methanol (2 mL) resulted in the formation of a green solution. Evaporation of solvent gave a green color powder (0.039 g, Yield 87%). ESI-MS (in CH_3OH) for $[\text{Ni}(\text{BPMCN})\text{Cl}]^+ (z=1)$ m/z 417.19 (experimental) m/z 417.14 (theoretical) and for $[\text{Ni}(\text{BPMCN})]^{2+} (z=2)$ m/z 191.25 (experimental) m/z 191.11 (theoretical). Elemental analysis Calculated (%): C 47.28, H 6.74, N 11.03, Cl 13.95 Found (%): C 47.45, H 6.51, N 11.51, Cl 14.78. UV-Vis λ_{max} in nm (ϵ in $\text{M}^{-1} \text{cm}^{-1}$) in MeOH at RT: 588 (13), 994 (13).

Synthesis of Ni(PDP)Cl₂ (4)

Similarly, when the ligand PDP (0.1 g, 3 mmol) dissolved in methanol (2 mL) was added dropwise to a stirring solution of $\text{NiCl}_2 \cdot 6\text{H}_2\text{O}$ (0.72 g, 3 mmol) in methanol (2 mL), a green solution was obtained. Evaporation of solvent gave a green color powder (0.271 g, Yield 83%). ESI-MS (in CH_3OH) for $[\text{Ni}(\text{BPMCN})\text{Cl}]^+ (z=1)$ m/z 415.19 (experimental) m/z 415.12 (theoretical) and for $[\text{Ni}(\text{BPMCN})]^{2+} (z=2)$ m/z 190.24 (experimental) m/z 190.01 (theoretical). Elemental analysis Calculated (%): C 51.1, H 6, N 11.92, Cl 15.08 Found (%): C 51.38, H 5.84, N 12.03, Cl 15.71. UV-Vis λ_{max} in nm (ϵ in $\text{M}^{-1} \text{cm}^{-1}$) in MeOH at RT: 581 (9), 976 (11).

Sample preparation and measurements

The UV-Vis absorption, emission and lifetime measurements were performed under anaerobic conditions at room temperature. A 1 mL solution of the MPA-CdTe QDs of concentration 1.4×10^{-6} M (0.5 mg mL^{-1}) in water was prepared. 30 mM stock solutions of the complexes **1–4** in water were also prepared. The MPA-CdTe QDs solutions were purged with nitrogen gas for 30 s in a micro cuvette (10 mm pathlength) whereas the Ni complexes **1–4** stock solutions were purged with nitrogen gas for 90 s.

To the MPA-CdTe QDs solution in the cuvette, an aliquot of 10 μL of the stock solution of **1** was added with the help of a gas tight syringe. Similar procedure was followed for the remaining complexes and all the measurements.

The cyclic voltammetry experiments were performed under a nitrogen atmosphere with Ag/AgCl as the reference electrode and 0.1 M KCl as the supporting electrolyte. To measure the potential of the MPA-CdTe QDs samples were scanned from -1.5 to $+1.5$ V in water with a scan rate varied from 100 to 500 mV s^{-1} . Similarly, the complexes were measured in water using a potential window of -1 V to $+1$ V with a scan rate varied from 100 to 500 mV s^{-1} .

Acknowledgements This work was funded by the University of Alabama in Huntsville, Individual Investigator Distinguished Research (IIDR) awards to Anusree Mukherjee and Seyed M. Sadeghi.

Compliance with ethical standards

Conflict of interest The authors declare no competing financial interest.

References

- Amelia M, Lincheneau C, Silvi S, Credi A (2012) Electrochemical properties of CdSe and CdTe quantum dots. *Chem Soc Rev* 41(17):5728–5743. <https://doi.org/10.1039/c2cs35117j>
- Anacona JR, Marquez VE, Jimenez Y (2009) Synthesis and characterization of manganese(II), nickel(II), copper(II) and zinc(II) Schiff-base complexes derived from 1,10-phenanthroline-2,9-dicarboxaldehyde and 2-mercaptoethylamine. *J Coord Chem* 62(7):1172–1179. <https://doi.org/10.1080/00958970802382768>
- Armaroli N, Balzani V (2007) The future of energy supply: challenges and opportunities. *Angew Chem Int Ed* 46(1+2):52–66. <https://doi.org/10.1002/anie.200602373>
- Artero V, Fontecave M (2013) Solar fuels generation and molecular systems: is it homogeneous or heterogeneous catalysis? *Chem Soc Rev* 42(6):2338–2356. <https://doi.org/10.1039/C2CS35334B>
- Bae Y, Myung N, Bard AJ (2004) Electrochemistry and electrogenerated chemiluminescence of CdTe nanoparticles. *Nano Lett* 4(6):1153–1161. <https://doi.org/10.1021/nl049516x>
- Berardi S, Drouet S, Francas L, Gimbert-Surinach C, Guttentag M, Richmond C, Llobet A (2014) Molecular artificial photosynthesis. *Chem Soc Rev* 43(22):7501–7519. <https://doi.org/10.1039/C3CS60405E>
- Brown KA, Dayal S, Ai X, Rumbles G, King PW (2010) Controlled assembly of hydrogenase-CdTe nanocrystal hybrids for solar hydrogen production. *J Am Chem Soc* 132(28):9672–9680. <https://doi.org/10.1021/ja101031r>
- Brown KA, Wilker MB, Boehm M, Dukovic G, King PW (2012) Characterization of photochemical processes for H₂ production by CdS nanorod-[FeFe] hydrogenase complexes. *J Am Chem Soc* 134(12):5627–5636. <https://doi.org/10.1021/ja2116348>
- Du P, Eisenberg R (2012) Catalysts made of earth-abundant elements (Co, Ni, Fe) for water splitting: recent progress and future challenges. *Energy Environ Sci* 5(3):6012–6021. <https://doi.org/10.1039/c2ee03250c>
- Esswein AJ, Nocera DG (2007) Hydrogen production by molecular photocatalysis. *Chem Rev* 107(10):4022–4047. <https://doi.org/10.1021/cr050193e>
- Fukuzumi S, Hong D, Yamada Y (2013) Bioinspired photocatalytic water reduction and oxidation with earth-abundant metal catalysts. *J Phys Chem Lett* 4(20):3458–3467. <https://doi.org/10.1021/jz401560x>
- Gaponik N, Talapin DV, Rogach AL, Hoppe K, Shevchenko EV, Kornowski A et al (2002) Thiol-capping of CdTe nanocrystals: an alternative to organometallic synthetic routes. *J Phys Chem B* 106(29):7177–7185. <https://doi.org/10.1021/jp025541k>
- Gimbert-Surinach C, Albero J, Stoll T, Fortage J, Collomb M-N, Deronzier A et al (2014) Efficient and limiting reactions in aqueous light-induced hydrogen evolution systems using molecular catalysts and quantum dots. *J Am Chem Soc* 136(21):7655–7661. <https://doi.org/10.1021/ja501489h>
- Greene BL, Joseph CA, Maroney MJ, Dyer RB (2012) Direct evidence of active-site reduction and photodriven catalysis in sensitized hydrogenase assemblies. *J Am Chem Soc* 134(27):11108–11111. <https://doi.org/10.1021/ja3042367>
- Gross MA, Reynal A, Durrant JR, Reisner E (2014) Versatile photocatalytic systems for H₂ generation in water based on an efficient DuBois-type nickel catalyst. *J Am Chem Soc* 136(1):356–366. <https://doi.org/10.1021/ja410592d>
- Guadalupe Hernandez HJ, Pandiyan T, Bernes S (2006) Mercaptoethanesulfonic acid (CoM imitator) interaction studies with nickel(II) complexes of pyridyl groups containing tetradentate ligands: synthesis, structure, spectra and redox properties. *Inorg Chim Acta* 359(1):1–12. <https://doi.org/10.1016/j.ica.2005.09.036>
- Gurumoorthy P, Mahendiran D, Kalilur Rahiman A (2016) Theoretical calculations, DNA interaction, topoisomerase I and phosphatidylinositol-3-kinase studies of water soluble mixed-ligand nickel(II) complexes. *Chem. Biol. Interact.* 248:21–35. <https://doi.org/10.1016/j.cbi.2016.02.002>
- Gust D, Moore TA, Moore AL (2001) Mimicking photosynthetic solar energy transduction. *Acc Chem Res* 34(1):40–48. <https://doi.org/10.1021/ar9801301>
- Haram SK, Kshirsagar A, Gujarathi YD, Ingole PP, Nene OA, Markad GB, Nanavati SP (2011) Quantum confinement in CdTe quantum dots: investigation through cyclic voltammetry supported by density functional theory (DFT). *J Phys Chem C* 115(14):6243–6249. <https://doi.org/10.1021/jp111463f>
- Helm ML, Stewart MP, Bullock RM, DuBois MR, DuBois DL (2011) A synthetic nickel electrocatalyst with a turnover frequency above 100,000 s⁻¹ for H₂ production. *Science* 333(6044):863–866. <https://doi.org/10.1126/science.1205864>
- Huang J, Mulfort KL, Du P, Chen LX (2012) Photodriven charge separation dynamics in CdSe/zns core/shell quantum dot/cobaloxime hybrid for efficient hydrogen production. *J Am Chem Soc* 134(40):16472–16475. <https://doi.org/10.1021/ja3062584>
- Kaerkaes MD, Verho O, Johnston EV, Aakermark B (2014) Artificial photosynthesis: molecular systems for catalytic water oxidation. *Chem Rev* 114(24):11863–12001. <https://doi.org/10.1021/cr400572f>
- Kalyanasundaram K, Graetzel M (2010) Artificial photosynthesis: biomimetic approaches to solar energy conversion and storage. *Curr Opin Biotechnol* 21(3):298–310. <https://doi.org/10.1016/j.copbio.2010.03.021>
- Kankanamalage PHA, Ekanayake DM, Singh N, de Morais ACP, Mazumder S, Verani CN, Mukherjee A, Lanznaster M (2019) Effect of ligand substituents on nickel and copper [N₄] complexes: electronic and redox behavior, and reactivity towards protons. *New J Chem.* <https://doi.org/10.1039/C9NJ01283D>
- Kilgore UJ, Roberts JAS, Pool DH, Appel AM, Stewart MP, DuBois MR et al (2011) [Ni(PPh₂NC₆H₄X₂)₂]²⁺ complexes as electrocatalysts for H₂ production: effect of substituents, acids, and water on catalytic rates. *J Am Chem Soc* 133(15):5861–5872. <https://doi.org/10.1021/ja109755f>
- Kim D, Sakimoto KK, Hong D, Yang P (2015) Artificial photosynthesis for sustainable fuel and chemical production. *Angew Chem Int Ed* 54(11):3259–3266. <https://doi.org/10.1002/anie.201409116>
- Li C-B, Li Z-J, Yu S, Wang G-X, Wang F, Meng Q-Y, Wu L-Z (2013a) Interface-directed assembly of a simple precursor of [FeFe]-H₂ase mimics on CdSe QDs for photosynthetic hydrogen evolution in water. *Energy Environ Sci* 6(9):2597–2602. <https://doi.org/10.1039/c3ee40992a>
- Li Z-J, Li X-B, Wang J-J, Yu S, Li C-B, Tung C-H, Wu L-Z (2013b) A robust “artificial catalyst” in situ formed from CdTe QDs and inorganic cobalt salts for photocatalytic hydrogen evolution. *Energy Environ Sci* 6(2):465–469. <https://doi.org/10.1039/C2EE23898E>
- Li Z-J, Fan X-B, Li X-B, Li J-X, Ye C, Wang J-J, Wu L-Z (2014) Visible light catalysis-assisted assembly of Ni-QD hollow nanospheres in situ via hydrogen bubbles. *J Am Chem Soc* 136(23):8261–8268. <https://doi.org/10.1021/ja5047236>

- Li X-B, Tung C-H, Wu L-Z (2018) Semiconducting quantum dots for artificial photosynthesis. *Nat Rev Chem* 2(8):160–173. <https://doi.org/10.1038/s41570-018-0024-8>
- Liu W, Migdisov A, Williams-Jones A (2012) The stability of aqueous nickel(II) chloride complexes in hydrothermal solutions: results of UV–Visible spectroscopic experiments. *Geochim Cosmochim Acta* 94:276–290. <https://doi.org/10.1016/j.gca.2012.04.055>
- Liu C, Qiu F, Peterson JJ, Krauss TD (2015) Aqueous photogeneration of H₂ with CdSe nanocrystals and nickel catalysts: electron transfer dynamics. *J Phys Chem B* 119(24):7349–7357. <https://doi.org/10.1021/jp510935w>
- Mao SS, Shen S (2013) Hydrogen production catalysing artificial photosynthesis. *Nat Photonics* 7(12):944–946. <https://doi.org/10.1038/nphoton.2013.326>
- Mautner FA, Mikuriya M, Ishida H, Sakiyama H, Louka FR, Humphrey JW, Massoud SS (2009) Dicyanamido-metal(II) complexes. Part 4: synthesis, structure and magnetic characterization of polynuclear Cu(II) and Ni(II) complexes bridged by μ -1,5-dicyanamide. *Inorg Chim Acta* 362(11):4073–4080. <https://doi.org/10.1016/j.ica.2009.05.066>
- Mulfort KL, Utschig LM (2016) Modular homogeneous chromophore-catalyst assemblies. *Acc Chem Res* 49(5):835–843. <https://doi.org/10.1021/acs.accounts.5b00539>
- Nann T, Ibrahim SK, Woi P-M, Xu S, Ziegler J, Pickett CJ (2010) Water splitting by visible light: a nanophotocathode for hydrogen production. *Angew Chem Int Ed* 49(9):1574–1577. <https://doi.org/10.1002/anie.200906262>
- Pella BJ, Niklas J, Poluektov OG, Mukherjee A (2018) Effects of denticity and ligand rigidity on reactivity of copper complexes with cumyl hydroperoxide. *Inorg Chim Acta* 483:71–78. <https://doi.org/10.1016/j.ica.2018.07.035>
- Poznyak SK, Osipovich NP, Shavel A, Talapin DV, Gao M, Eychmueller A, Gaponik N (2005) Size-dependent electrochemical behavior of thiol-capped CdTe nanocrystals in aqueous solution. *J Phys Chem B* 109(3):1094–1100. <https://doi.org/10.1021/jp0460801>
- Rajh T, Micic OI, Nozik AJ (1993) Synthesis and characterization of surface-modified colloidal cadmium telluride quantum dots. *J Phys Chem* 97(46):11999–12003. <https://doi.org/10.1021/j100148a026>
- Sadeghi SM, Wing WJ, Gutha RR, Wilt JS, Wu JZ (2018) Balancing silicon/aluminum oxide junctions for super-plasmonic emission enhancement of quantum dots via plasmonic metafilms. *Nanoscale* 10(10):4825–4832. <https://doi.org/10.1039/C7NR09396A>
- Sadeghi SM, Wing WJ, Gutha RR, Goul RW, Wu JZ (2019) Functional metal-oxide plasmonic metastructures: ultrabright semiconductor quantum dots with polarized spontaneous emission and suppressed Auger recombination. *Phys Rev Appl* 11(2):024045. <https://doi.org/10.1103/PhysRevApplied.11.024045>
- Sadhu MH, Solanki A, Kumar SB (2015) Mixed ligand complexes of copper(II), cobalt(II), nickel(II) and zinc(II) with thiocyanate and pyrazole based tetradentate ligand: syntheses, characterizations and structures. *Polyhedron* 100:206–214. <https://doi.org/10.1016/j.poly.2015.07.067>
- Shi L, Hernandez B, Selke M (2006) Singlet oxygen generation from water-soluble quantum dot-organic dye nanocomposites. *J Am Chem Soc* 128(19):6278–6279. <https://doi.org/10.1021/ja057959c>
- Silver SC, Niklas J, Du P, Poluektov OG, Tiede DM, Utschig LM (2013) Protein delivery of a Ni catalyst to photosystem I for light-driven hydrogen production. *J Am Chem Soc* 135(36):13246–13249. <https://doi.org/10.1021/ja405277g>
- Singh N, Niklas J, Poluektov O, Van Heuvelen KM, Mukherjee A (2017) Mononuclear nickel(II) and copper(II) coordination complexes supported by bispicen ligand derivatives: experimental and computational studies. *Inorg Chim Acta* 455(Part_1):221–230. <https://doi.org/10.1016/j.ica.2016.09.001>
- Utschig LM, Soltau SR, Tiede DM (2015) Light-driven hydrogen production from photosystem I-catalyst hybrids. *Curr Opin Chem Biol* 25:1–8. <https://doi.org/10.1016/j.cbpa.2014.11.019>
- Vullev VI (2011) From biomimesis to bioinspiration: what's the benefit for solar energy conversion applications? *J Phys Chem Lett* 2(5):503–508. <https://doi.org/10.1021/jz1016069>
- Wang X, Li C (2017) Interfacial charge transfer in semiconductor-molecular photocatalyst systems for proton reduction. *J Photochem Photobiol C* 33:165–179. <https://doi.org/10.1016/j.jphotochemrev.2017.10.003>
- Wang F, Wang W-G, Wang X-J, Wang H-Y, Tung C-H, Wu L-Z (2011) A highly efficient photocatalytic system for hydrogen production by a robust hydrogenase mimic in an aqueous solution. *Angew Chem Int Ed* 50(14):3193–3197. <https://doi.org/10.1002/anie.201006352> (S3193/3191–S3193/3116)
- Wang D, Zhang Y, Chen W (2014) A novel nickel-thiourea-triethylamine complex adsorbed on graphitic C₃N₄ for low-cost solar hydrogen production. *Chem Commun* 50(14):1754–1756. <https://doi.org/10.1039/c3cc48141g>
- Wang M, Han K, Zhang S, Sun L (2015) Integration of organometallic complexes with semiconductors and other nanomaterials for photocatalytic H₂ production. *Coord Chem Rev* 287:1–14. <https://doi.org/10.1016/j.ccr.2014.12.005>
- Wen F, Li C (2013) Hybrid artificial photosynthetic systems comprising semiconductors as light harvesters and biomimetic complexes as molecular cocatalysts. *Acc Chem Res* 46(11):2355–2364. <https://doi.org/10.1021/ar300224u>
- Wilson AD, Newell RH, McNevin MJ, Muckerman JT, Rakowski DuBois M, DuBois DL (2006) Hydrogen oxidation and production using nickel-based molecular catalysts with positioned proton relays. *J Am Chem Soc* 128(1):358–366. <https://doi.org/10.1021/ja056442y>
- Wilson AD, Shoemaker RK, Miedaner A, Muckerman JT, DuBois DL, Dubois MR (2007) Nature of hydrogen interaction with Ni(II) complexes containing cyclic phosphine ligands with pendant nitrogen bases. *Proc Natl Acad Sci USA* 104(17):6951–6956. <https://doi.org/10.1073/pnas.0608928104>
- Wu L-Z, Chen B, Li Z-J, Tung C-H (2014) Enhancement of the efficiency of photocatalytic reduction of protons to hydrogen via molecular assembly. *Acc Chem Res* 47(7):2177–2185. <https://doi.org/10.1021/ar500140r>
- Xu Y, Zhang B (2015) Hydrogen photogeneration from water on the biomimetic hybrid artificial photocatalytic systems of semiconductors and earth-abundant metal complexes: progress and challenges. *Catal Sci Technol* 5(6):3084–3096. <https://doi.org/10.1039/C5CY00365B>
- Yu WW, Qu L, Guo W, Peng X (2003) Experimental determination of the extinction coefficient of CdTe, CdSe, and CdS nanocrystals. *Chem Mater* 15(14):2854–2860. <https://doi.org/10.1021/cm034081k>
- Zhang H, Zhou Z, Yang B, Gao M (2003) The influence of carboxyl groups on the photoluminescence of mercaptocarboxylic acid-stabilized CdTe nanoparticles. *J Phys Chem B* 107(1):8–13. <https://doi.org/10.1021/jp025910c>
- Zhou H, Yan R, Zhang D, Fan T (2016) Challenges and perspectives in designing artificial photosynthetic systems. *Chem Eur J* 22(29):9870–9885. <https://doi.org/10.1002/chem.201600289>
- Zhou Y, Yang S, Huang J (2017) Light-driven hydrogen production from aqueous solutions based on a new Dubois-type nickel catalyst. *Phys Chem Chem Phys* 19(11):7471–7475. <https://doi.org/10.1039/C7CP00247E>
- Zilbermann I, Maimon E, Cohen H, Meyerstein D (2005) Redox chemistry of nickel complexes in aqueous solutions. *Chem Rev* 105(6):2609–2626. <https://doi.org/10.1021/cr030717f>

Publisher's Note Springer Nature remains neutral with regard to jurisdictional claims in published maps and institutional affiliations.

Affiliations

Niharika Krishna Botcha¹ · Rithvik R. Gutha² · Seyed M. Sadeghi² · Anusree Mukherjee¹

✉ Anusree Mukherjee
anusree.mukherjee@uah.edu

² Department of Physics and Astronomy, The University of Alabama in Huntsville, 301 Sparkman Drive, Huntsville, AL 35899, USA

¹ Department of Chemistry, The University of Alabama in Huntsville, 301 Sparkman Drive, Huntsville, AL 35899, USA